KERNFORSCHUNGSANLAGE JÜLICH GmbH
Institut für Nukleare Sicherheitsforschung

AN EXPERIMENTAL INVESTIGATION ON MASS TRANSFER IN PRESENCE OF CHEMICAL REACTIONS ON A GRAPHITE CYLINDER IN CROSSFLOW

by
M. Ogawa, B. Stauch, R. Moormann, W. Katscher

Jül-Spez-336
November 1985
ISSN 0343-7639

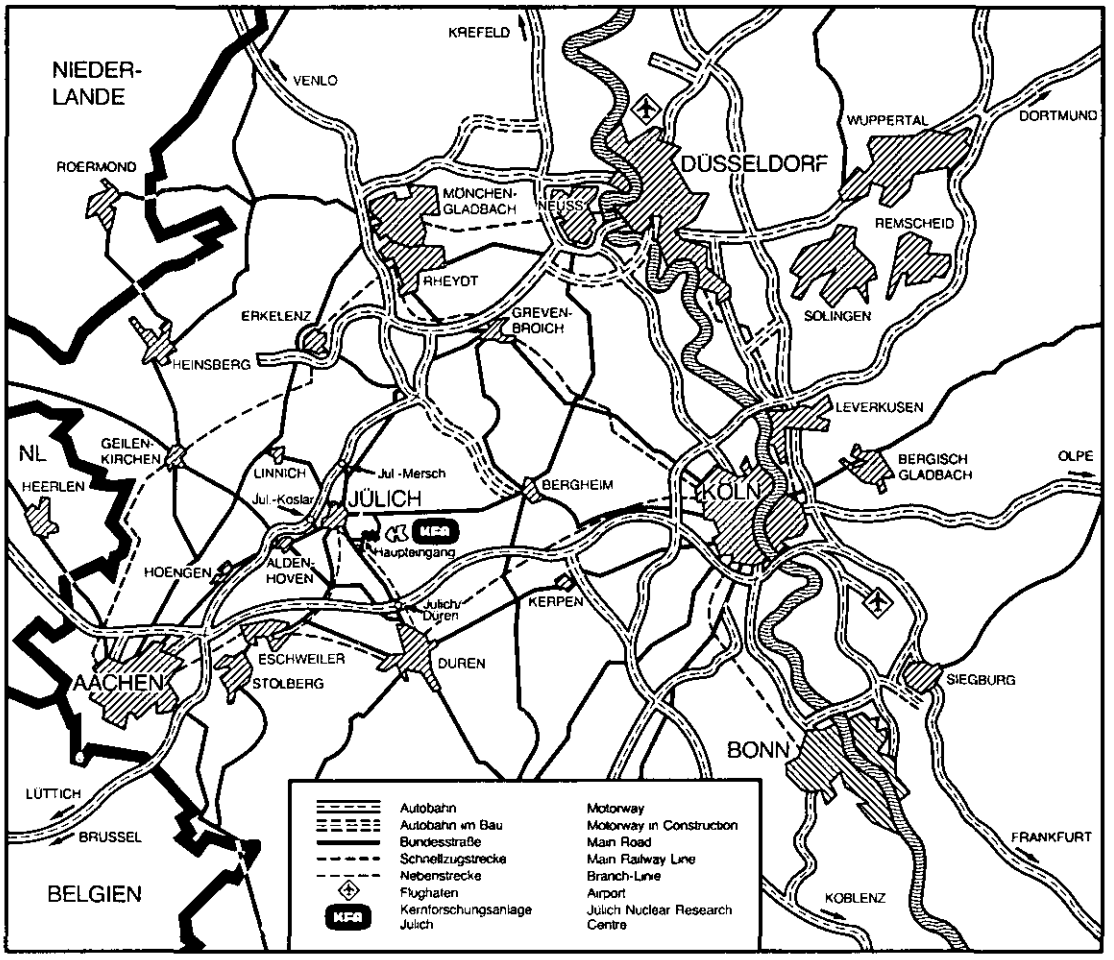

Als Manuskript gedruckt

Spezielle Berichte der Kernforschungsanlage Jülich – Nr. 336
Institut für Nukleare Sicherheitsforschung Jül-Spez-336

Zu beziehen durch: ZENTRALBIBLIOTHEK der Kernforschungsanlage Jülich GmbH
Postfach 1913 · D-5170 Jülich (Bundesrepublik Deutschland)
Telefon: 02461/610 · Telex: 833556-0 kf d

AN EXPERIMENTAL INVESTIGATION ON MASS TRANSFER IN PRESENCE OF CHEMICAL REACTIONS ON A GRAPHITE CYLINDER IN CROSSFLOW

by
M. Ogawa, B. Stauch, R. Moormann, W. Katscher

CONTENTS

ABSTRACT

In connection with analyses of hypothetical massive air ingress accidents in HTGR (High Temperature Gas-Cooled Reactor), in which it is assumed that the air is transported through the hot region of graphite core support posts, experiments on mass transfer and in-pore diffusion with homogeneous and heterogeneous chemical reactions were performed on a graphite cylinder in crossflow. Two BLMR (Boundary Layer Mass transfer controlled Regime) runs and two runs in an intermediate regime between BLMR and IPDR (In-Pore-Diffusion controlled Regime) were executed at atmospheric pressures, Reynolds numbers ranging from 533 to 2490, and cylinder temperatures from 848°C to 1120°C. The nuclear grade graphite cylinder having a diameter of 100 mm and a porosity of 21.2 % was corroded in a nitrogen gas flow containing approximately 5 % oxygen. Mean and local mass transfer coefficients and corrosion rates were obtained to examine the influences of the chemical reactions on the mass transfer. As a result it can be concluded that the chemical reactions and small changes in shape do not significantly influence the mass transfer under conditions to be expected in HTGR air ingress accidents and that thus the analogy between heat and mass transfer can be used for safety calculations.

1. INTRODUCTION

The investigation on the corrosion of a graphite cylinder by oxygen at high temperatures was carried out in connection with analyses of hypothetical air ingress accidents in high temperature gas cooled reactors (HTGR) which - following analyses on the more probable water ingress accidents /1,2/ - have been accomplished during recent years.

The most important chemical reactions between the air entering the primary circuit and the hot graphite are the heterogeneous reactions

$$C + xO_2 \longrightarrow yCO + zCO_2 \qquad (1\text{-}1)$$

$$C + CO_2 \rightleftharpoons 2CO \qquad (1\text{-}2)$$

and the homogeneous reaction

$$2CO + O_2 \longrightarrow 2CO_2 \qquad (1\text{-}3)$$

Depending on the temperature, the reaction between a porous solid like graphite and a corrosive gas like oxygen with gaseous products reveals three characteristic regimes /3/, as shown schematically in Fig. 1.

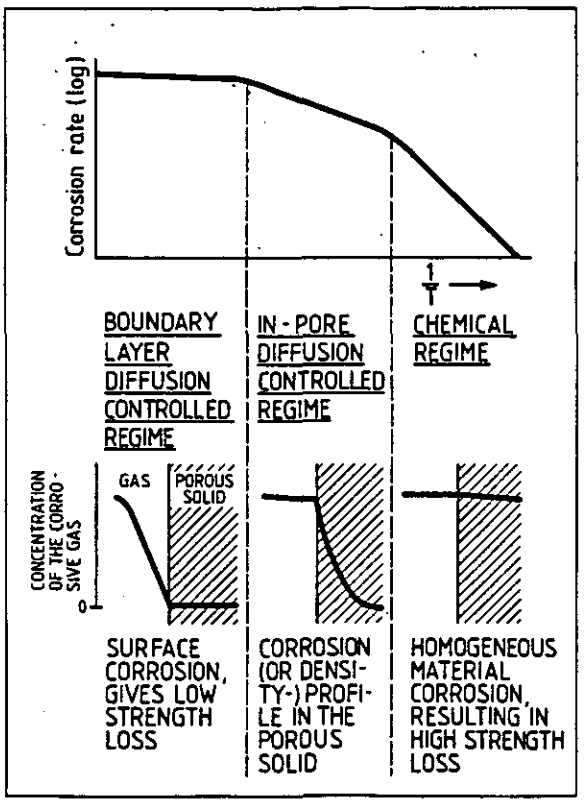

Fig. 1: Scheme of reactions between gases and porous solids with exclusively gaseous products

At low temperatures - in our case below approx. 500°C - the chemical reaction is so slow that the oxygen can penetrate the pore system of the graphite in depth with only a small concentration gradient. The corrosion attack is fairly uniform throughout the material. This is called the chemical regime (CR). Towards higher temperatures (and thus increasing chemical reactivity) - up to approx. 900°C - the corrosion process is strongly influenced by gas diffusion processes in the pore system. The concentration profile of the corroding gas becomes steeper with increasing temperatures: the corrosion attack is more or less restricted to the narrow zone close to the surface of the graphite body. This is the in-pore diffusion controlled regime (IPDR). At higher temperatures - above approx. 900°C - the chemical reactivity is so high that the reaction is practically exclusively observed at the surface of the graphite. Mass transfer in the gas phase to and from the graphite surface becomes the determining processes, so that this regime may be called the boundary layer mass transfer controlled regime (BLMR).

Especially the latter two regimes are important for accident analyses and thus their kinetics are incorporated in the computer code REACT/THERMIX /4/, which was developed for analyses of air and water ingress accidents in pebble bed HTGR /5,6/. In the IPDR the code uses material specific corrosion rates which were measured as functions of graphite temperatures, oxygen partial pressure and burnoff /7-10/. In the BLMR the analogy between heat and mass transfer /11/ was taken as valid, which here opens applicability of a great number of heat transfer investigations (e.g. /12-25/) to the corrosion calculations. The feasibility of the analogy between heat and mass transfer for graphite corrosion processes in the BLMR is based on the assumption that the chemical reactions do not influence the mass transfer. That this assumption might not apply, however, recently was reported by Specht and Jeschar /26/. They investigated the coupling of convection and chemical kinetics on burning carbon particles and found out that the burn-off rate might be increased up to a factor of about 3 by the chemical reaction. This is possibly explained mainly by a model, where the oxygen is consumed in the boundary layer by the homogenous reaction (1-3), and the heterogeneous reaction is only the Boudouard reaction (1-2). This mechanism will lead to a steeper gradient of the reacting gas in the boundary layer than by simple mass transfer assumptions. Consequently, the diffusional mass transfer is promoted. Additional effects are caused by the temperature distribution in the boundary layer with a pronounced maximum in the region of the homo-

geneous reaction.

In order to examine whether such a reaction induced increase of the reaction rate in the BLMR also would take place under the air ingress accident conditions mentioned above experiments were carried out using graphite cylinders corroded in a O_2/N_2 mixture at temperatures between 850°C and 1100°C in cross-flow with Reynolds numbers ranging from approx. 530 to 2500. The cylinder was chosen as a simple geometry offering good comparability to heat transfer experiments, simultaneously also in form of core support posts being part of the core support structure of various modern HTGR designs. The parameters were chosen from those used in accident calculations which were carried out for the case of direct air ingress into the hot gas plenum of a process heat generating HTGR /27/ taking into account the limitations of the test facility available.

2. EXPERIMENTAL

2.1 The test facility

The experiments were carried out in the test facility SUPERNOVA /28/, which was constructed for corrosion experiments on graphite pebble beds under conditions simulating severe air or steam ingress accidents in HTGR cores.

As shown schematically in Fig. 2, the main components of SUPERNOVA are an electrically heated tube furnace incorporating the test section, a gas preheater, a gas supply system and measuring and data collecting systems.

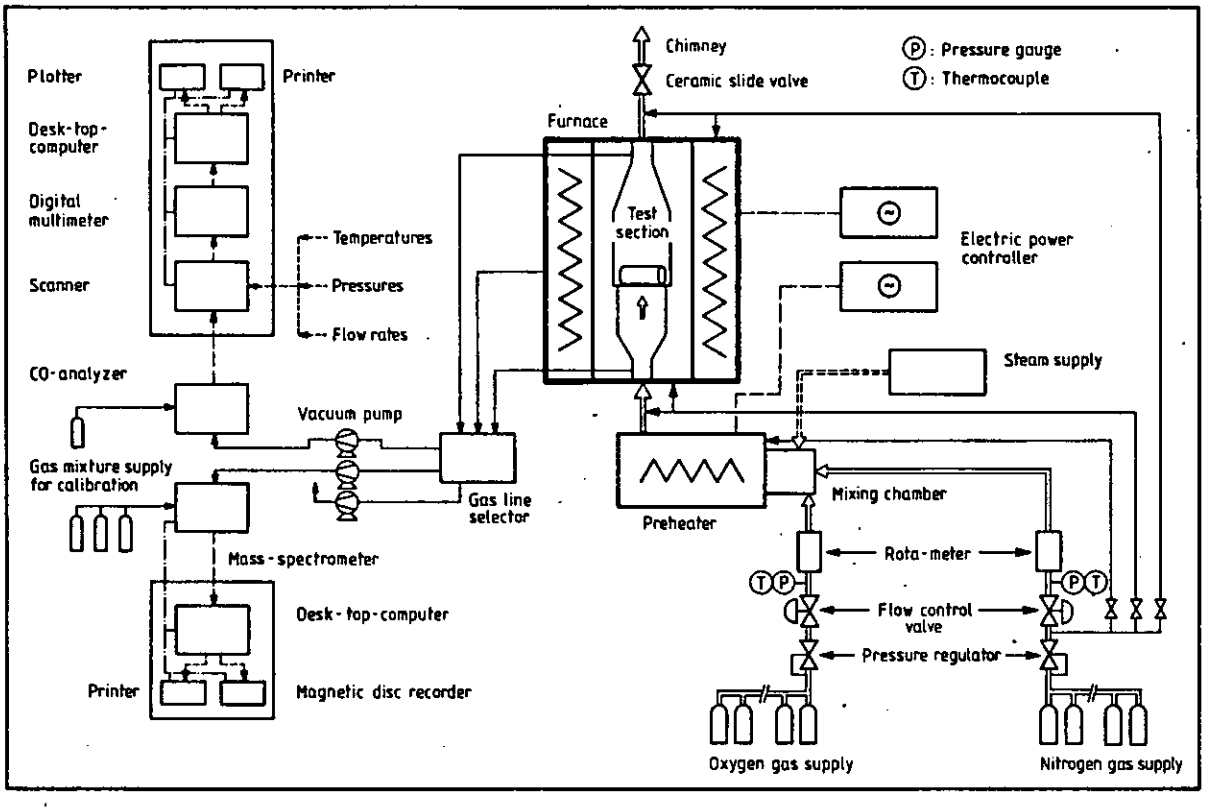

Fig. 2: Flow diagram of graphite corrosion experimental facility SUPERNOVA

The gas supply system can deliver a maximum of 250 Nm^3/h nitrogen and oxygen from compressed gas bottles. The gases are mixed in a mixing chamber and passed through the gas preheater where they can be heated to a maximum temperature of 1200°C. The gas mixture is then passed through the test section

and released to the environment through a chimney.

Fig. 3 shows the test section in the furnace. The furnace can be heated to a max. temperature of 1500°C. The test section ("outer ceramic tube") consists of a silica tube with an inner diameter of 350 mm and a height of 900 mm with multi hole plates at the inlet and outlet ends. These plates serve as flow restrictors during the heating or cooling period of the test section, when nitrogen at a low flow rate (10 m^3/h) is blown into the test section close to the lower end. The nitrogen separates into two streams which leave the test section through the two multi hole plates, thus preventing corrosive gases (rests of moisture or oxygen) from entering the test section and from causing uncontrolled oxidation of the graphite test specimen. In this test section a second tube ("inner ceramic tube") is positioned as shown in Fig. 3. This tube has an inner diameter of 290 mm and a height of 280 mm. At the lower end an additional multi hole plate is placed for flow equalization. The graphite cylinder sets on top of the inner tube. The test section is equipped with 10 chromel-alumel thermocouples for wall and gas temperature measurements as shown in Fig. 3.

Also indicated in this figure are the different tappings in the furnace for gas concentration and pressure measurements.

The graphite cylinder is shown in Fig. 4. It has a diameter typical for HTGR core support posts and is made of the graphite V483T manufactured by the Ringsdorff-Werke in Bonn. V483T contains a pitch coke filler and pitch binder. It is manufactured by isostatic moulding and graphitized at 2800°C. The nominal bulk density is 1780 kg/m^3, the total ash content is less than 250 ppm. The cylinder could be equipped with 9 thermocouples (positions shown in Fig. 4). The center bore which was closed by a plug during the experiments, was used as the reference for radius measurements of the corroded samples (see 2.2).

The temperatures in the test section and gas temperatures at the flow meters were measured with chromel-alumel thermocouples, the preheater and furnace temperatures were measured with platinium-rhodium thermocouples.

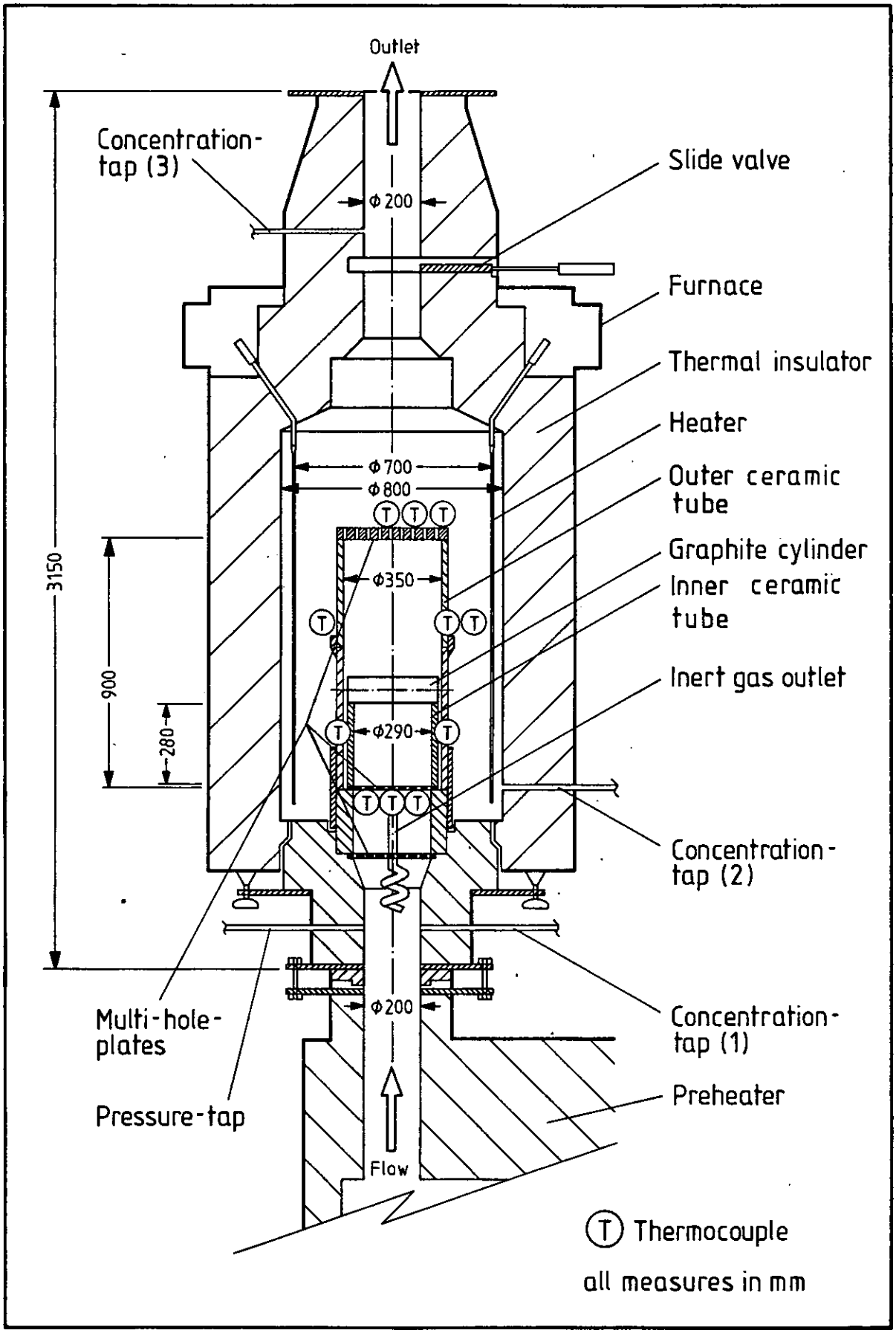

Fig. 3: Tube furnace with test section

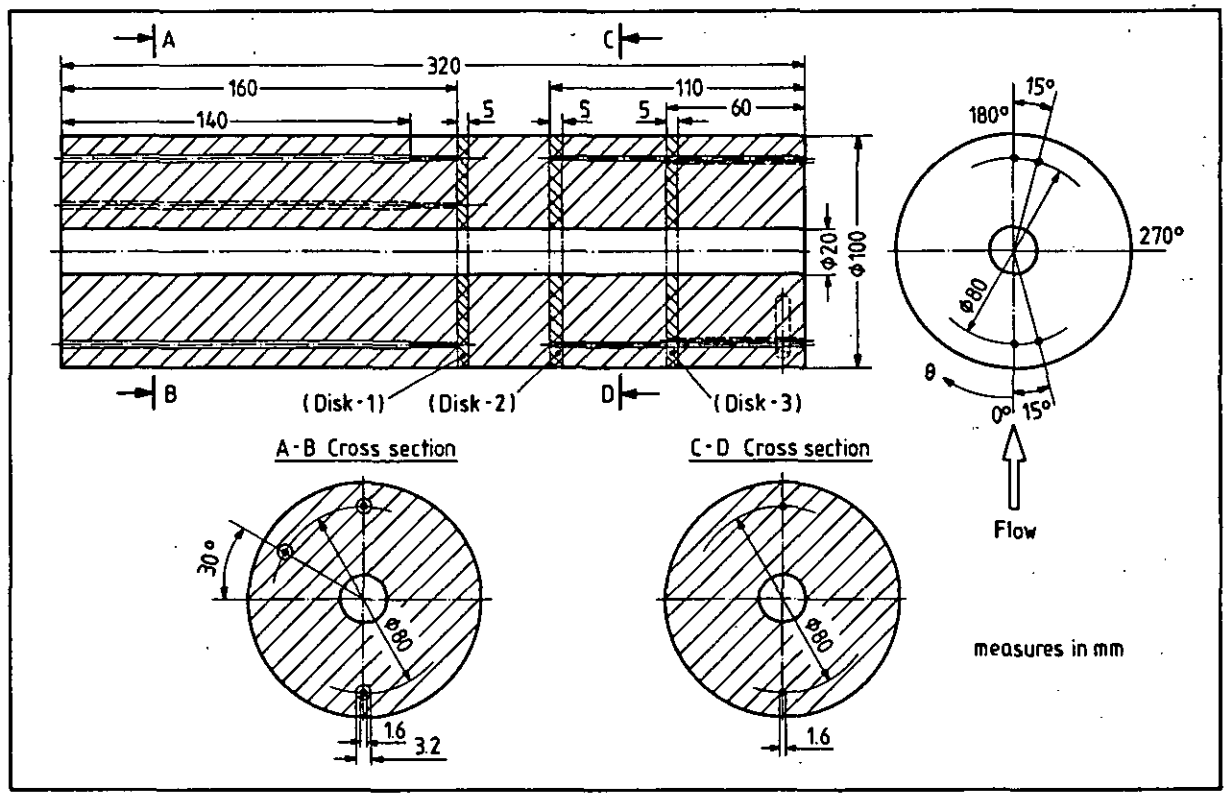

Fig. 4: Graphite cylinder

The nitrogen and oxygen flow rates were measured with rotameters (flow range N_2: 26-260 Nm^3/h, flow range O_2: 0.7-70 Nm^3/h, accuracy ±5 %). These flow meters were equipped with electrical transducers.

The pressure of the gas mixture at the test section inlet and of the nitrogen and oxygen at the rotameters were measured with capacitive pressure transducers (type SETRA 0-1.7237·10^5 Pa, output 0-5 V, accuracy 0.1 %).

The oxygen and carbon dioxide concentrations at the inlet and the outlet of the test section and in the furnace were measured by a mass-spectrometer (QUADRUVAC Q 200, Leybold-Heraeus), controlled by a desk top computer data acquisition system (APPLE-CIFMAC); the concentration of carbon monoxide was measured by a CO-analyzer (URAS 3, made by Hartmann & Braun Co., range 0-1000 ppm and 0-5 v/o).

All data, except the output of the mass spectrometer which was stored by the APPLE computer, were collected by a Hewlett-Packard data acquisition system (HP 3052A).

2.2 Experimental procedures and conditions

Before each test run the mass and the dimensions of the graphite cylinder were measured. After that, the cylinder was fixed in the test section and the thermocouples were mounted at the temperature measuring points in the cylinder and the inside and outside of the test-section.

The test section was placed in the furnace and the measuring instruments (thermocouples, pressure indicators and flow meters) were connected with the Hewlett-Packard data-acquisition system.

The mass-spectrometer and the CO-analyzer were calibrated before each run and periodically during the test by using standard gas mixtures containing oxygen, CO_2 and CO.

After these preparations, pure nitrogen gas was blown through the preheater and test section with a flow rate of approx. 100 m^3/h for about 20 minutes until the oxygen concentration, measured by mass spectrometer, decreased to less than 1 v/o.

Then the nitrogen flow rate was decreased to 10 m^3/h and directly blown into the test section as described in 2.1, while the slide valve at the outlet of the furnace was partly closed. The electrical heaters of the furnace and the gas preheater were switched on. Both heaters were heated up automaticly. The temperatures were measured with the data acquisition system and some representative temperature vs. time curves of the test section and the furnaces were drawn on a plotter.

When the temperatures of the graphite cylinder and the gas preheater reached the desired level and became steady state, the slide valve was opened, the nitrogen was passed through the gas preheater and the test section and its flow rate was increased to the desired level. The electric power of the furnace and gas preheater were controlled so that the inlet gas temperature of the test section and the cylinder temperatures became egual and steady

state. Then oxygen gas was mixed into the nitrogen flow and the total flow rate was regulated so that the oxygen volume concentrations became 5 v/o. The corrosion run was started. The experimental conditions were held for a certain testing time as listed in Table 1.

After the test-run, the oxygen flow was stopped, and nitrogen was blown directly into the test section in the same manner as during the heating-up-time. All heaters were switched off and the temperatures of the test section decreased.

When the graphite temperatures reached a value below 400°C, the test section was removed from the furnace. The graphite cylinder was weighed and sliced into three disks (designated as Disk 1,- 2 and 3) with a thickness of 5 mm as shown in Fig. 5. The mass of each disk was measured with a chemical balance, type METTLER AE 163 with a accuracy of 0.01 mg.

The circumferential decreases of radii were measured by a electronic linear gauge type MITUTOYO 542-101 with a accuracy of ± 1μm.

Parameter \ Run	1	2	3	4
Reynolds number	533	904	1660	2490
Oxygen concentration (%)	5.38	4.62	4.82	4.89
Pressure at test section x 10^5(Pa)	1.013	0,989	1.019	1.023
Average gas temperature (°C)	1100	875	1030	823
Average cylinder temperature (°C)	1120	910	1070	848
Average wall temperature (°C)	1110	893	1040	822
Duration of corrosion experiment (h)	5.00	5.00	2.25	3.00

Table 1: Experimental Conditions

3. EXPERIMENTAL RESULTS AND DISCUSSIONS

3.1 Oxidation of the graphite cylinder

3.1.1 Changes in shape

In a visual oberservation of the cylinder surface after corrosion, the appearance of the surface in Run 4 could be obviously distinguished from those in other runs. In detail, the surface of the cylinder in Run 4 was soft and was easily damaged, especially in the lower part (near the stagnation point). In other runs the cylinders were hard enough not to be damaged.

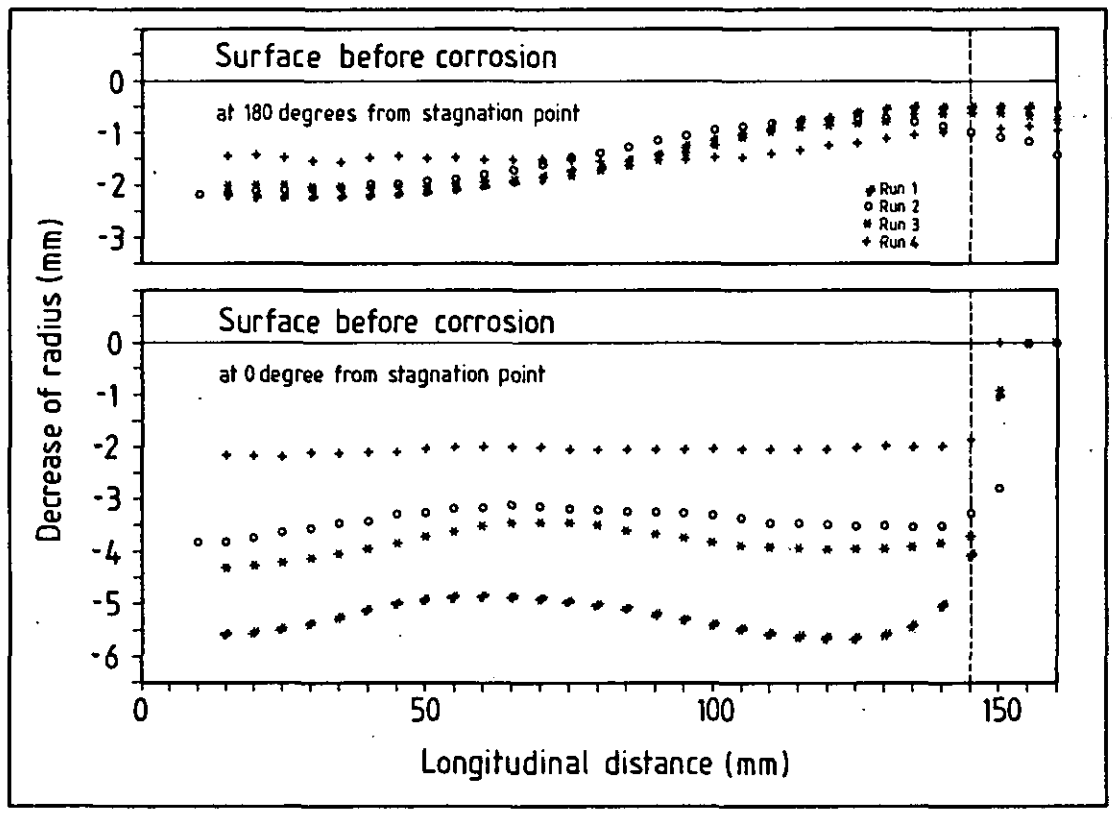

Fig. 5: Post corrosion longitudinal deformation of a graphite cylinder at 0° and 180° from stagnation point

Longitudinal decreases of radii of the cylinders in all runs are shown in

Fig. 5. The abscissa is a longitudinal distance of the cylinder and the ordinate is the decrease of radius measured from the original surface of the cylinder. The lower figure shows the decreases of radii at an angle of 0 degree from the stagnation point and the upper one at an angle of 180 degrees. It is found for the 0 degree case that the distribution of the decreases of radii becomes more uniform for bigger Reynolds numbers. The profile of the decreases of radii at 180 degrees seems to be influenced by the extention of the flow from the inner tube to the outer one. It was observed that these longitudinal distributions were symmetric with respect to the center of the test section.

The distributions of circumferential decreases of radii of each disk are shown in Figs. 6.1-6.4. The decreases of radii were measured at an angle interval of 5 degrees for Disk-1 and at an angle interval of 10 degrees for Disks-2 and -3. In volume calculations of the corroded disks by Eq. (3-1) the angle intervals $\Delta\Theta$ of 5, 10 and 15 degrees had little influence on the absolute value of the volume. Therefore the angle interval of 5 degrees only was adopted for Disk-1 and 10 degrees intervals were selected for Disks-2 an -3 to simplify the task of taking the measurements. In Figs. 6.1-6.4 the measured points are connected by straight lines. These changes in shape depend upon the distributions of local mass transfer coefficients. From Figs. 6.1-6.3 it is seen that the circumferential distributions were slightly

Figs. 6.1-6.4: Circumferential distribution of the radius decrease of the corroded graphite cylinders

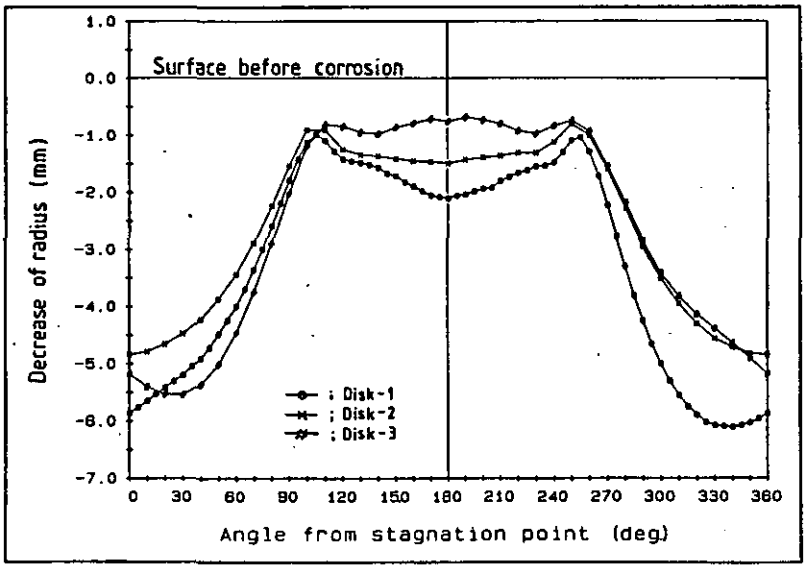

Fig. 6.1: Run 1

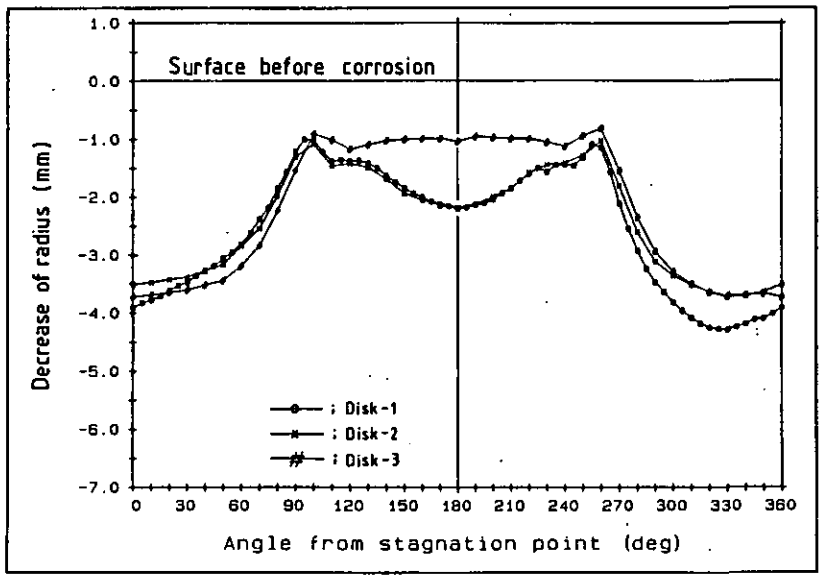

Fig. 6.2: Run 2

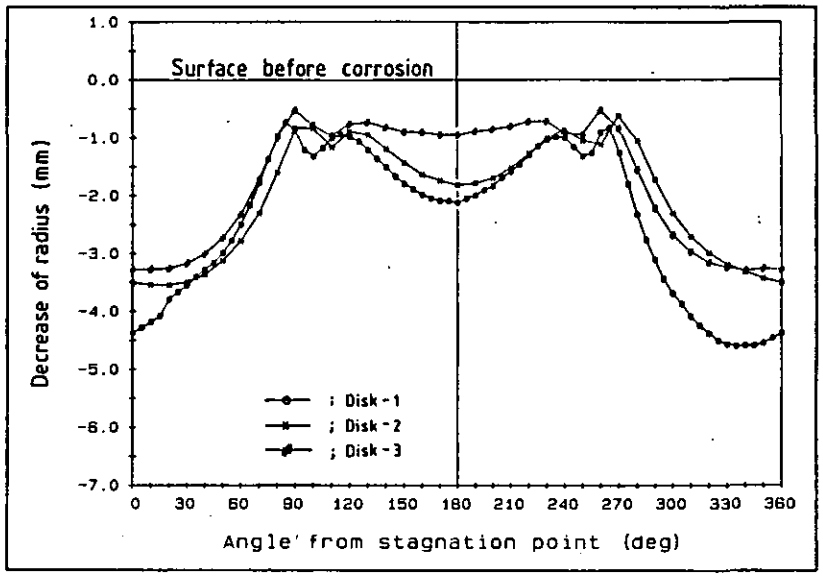

Fig. 6.3: Run 3

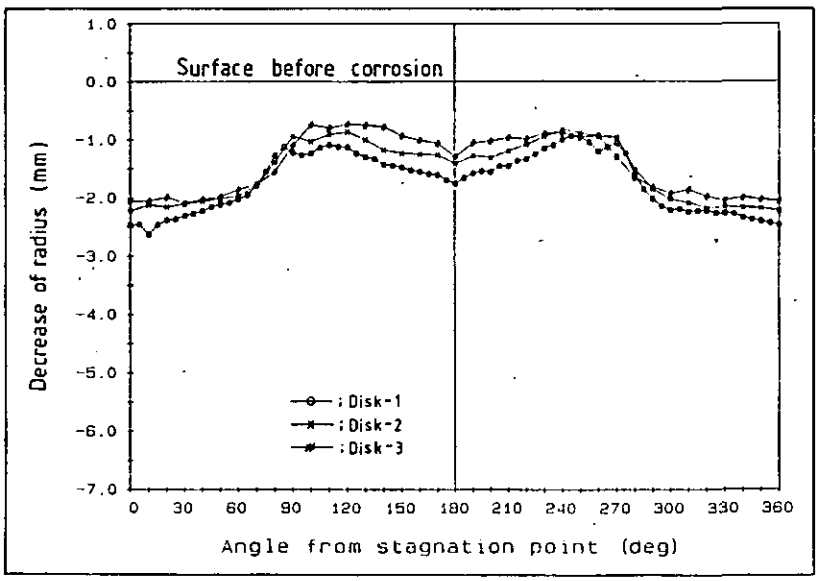

Fig. 6.4: Run 4

unsymmetric, especially in case of Disk-1. From Fig. 6.4 it appears that Run 4, as expected, was in the intermediate regime between IPDR and BLMR, because the profile of the decreases of radii for Run 4 was more uniform than those of the other runs. A fully uniform circumferential radius decrease would be expected only, if the corrosion took place exclusively in the IPDR.

3.1.2 Mass balances in the chemical reactions

The volume of the disk after corrosion $V_{cor,cal}$ was calculated by using the radii measured at each circumferential point as follows:

$$V_{cor,cal} = l\left[\int_0^{2\pi}\int_0^{r'} r\,dr\,d\theta - \pi r_{in}^2\right]$$

$$= \sum_{i=1}^{n} \Delta V_{cor,cal,\theta_i} - l\pi r_{in}^2$$

$$\Delta V_{cor,cal,\theta_i} = l\int_{\theta_i-\Delta\theta/2}^{\theta_i+\Delta\theta/2}\int_0^{\bar{r}} r\,dr\,d\theta$$

$$= \frac{l\Delta\theta}{2}\left(r_i + \frac{c_1}{12}\Delta\theta^2\right)^2$$

$$r = c_1\theta^2 + c_2\theta + c_3$$

$$c_1 = \frac{\begin{vmatrix} r_{i-1} & \theta_{i-1} & 1 \\ r_i & \theta_i & 1 \\ r_{i+1} & \theta_{i+1} & 1 \end{vmatrix}}{\begin{vmatrix} \theta_{i-1}^2 & \theta_{i-1} & 1 \\ \theta_i^2 & \theta_i & 1 \\ \theta_{i+1}^2 & \theta_{i+1} & 1 \end{vmatrix}}$$

$$\bar{r} = \frac{\int_{\theta_i-\Delta\theta/2}^{\theta_i+\Delta\theta/2} r\,d\theta}{\int_{\theta_i-\Delta\theta/2}^{\theta_i+\Delta\theta/2} d\theta}$$

(3-1)

where $\Delta V_{cor,cal,\theta i}$ was the partial volume of the disk after corrosion from the angle of $(\theta_i - \Delta\theta/2)$ to $(\theta_i + \Delta\theta/2)$, r_i the radius measured at the angle of θ_i, and r_{in} the inner radius of the disk.

Variations of the mass due to graphite corrosion are listed in Table 2. The mass of the disk before corrosion was calculated from the following equation:

$$m_o = V_o \cdot \rho_{b,o} \tag{3-2}$$

where V_o was evaluated from the diameter of the cylinder measured before corrosion and the thickness of the disk after the slicing. Two masses of the disks after corrosion were obtained: $m_{cor,ms}$ by weight measurements and $m_{cor,cal}$ by the following equation:

$$m_{cor,cal} = V_{cor,cal} \cdot \rho_{b,o} \tag{3-3}$$

Accordingly, two kinds of corroded masses $\Delta m_v^{(1)}$ and $\Delta m_c^{(2)}$ were obtained from Eqs. (3-4) and (3-5).

$$m_c^{(1)} = m_o - m_{cor,ms} \tag{3-4}$$

$$m_c^{(2)} = m_o - m_{cor,cal} \tag{3-5}$$

In the results of Table 2 there is a tendency that calculated masses after corrosion $m_{cor,cal}$ are slightly greater than the measured values $m_{cor,ms}$ for all disks. This tendency indicates that slight in-pore corrosion took place, even in BLMR. An average depth of the corrosion attack in the graphite due to the in-pore diffusion $\overline{\Delta r}_{cor,IPD}$ can be defined by Eq. (3-6).

$$\overline{\Delta r}_{cor,IPDR} = \frac{(\Delta m_c^{(1)} \cdot \Delta m_c^{(2)})}{2 \cdot \pi \cdot \bar{r} \cdot 1 \cdot \bar{\rho}_{b,o,cor}} \tag{3-6}$$

where $\bar{r}$ denoted the radius of the disk averaged circumferentially after corrosion and $\overline{\rho}_{b,o,cor}$ the average bulk density in the region attacked by the in-pore corrosion. With the assumption that $\overline{\rho}_{b,o,cor}$ is equal to $\rho_{b,o}/2$, $\overline{\Delta r}_{cor,IPD}$ is calculated and tabulated in Table 2.

Value \ Run	Disk	1	2	3	4
Bulk density of the graphite before corrosion ; $\rho_{b,0}$ (kg/m^3)		1786	1783	1776	1780
Mass of the disk before corrosion ; m_0 ($=V_0 \times \rho_{b,0}$) (g)	1	67.26	66.59	66.34	67.25
	2	66.77	66.92	66.87	66.98
	3	67.33	67.31	66.94	66.94
Mass of the disk measured after corrosion ; $m_{cor,ms}$ (g)	1	58.04	59.32	59.48	62.15
	2	59.32	60.08	61.12	61.71
	3	59.63	60.91	61.71	62.40
Calculated mass of the disk after corrosion; $m_{cor,cal}$ (g)	1	58.70	59.82	59.95	62.57
	2	59.96	60.43	61.46	62.82
	3	60.46	61.48	62.26	63.06
Corroded mass of the disk ; $\Delta m_C^{(1)}$ ($=m_0 - m_{cor,ms}$) (weighed) (g)	1	9.22	7.27	6.86	5.10
	2	7.45	6.83	5.75	5.27
	3	7.70	6.40	5.22	4.54
Corroded mass of the disk ; $\Delta m_C^{(2)}$ ($=m_0 - m_{cor,cal}$) (calculated) (g)	1	8.56	6.77	6.39	4.68
	2	6.81	6.49	5.41	4.16
	3	6.87	5.83	4.68	3.88
Average depth of corrosion attack ; $\overline{\Delta r_{cor,IPD}}$ (mm)	1	0.12	0.09	0.09	0.08
	2	0.12	0.06	0.06	0.21
	3	0.16	0.11	0.10	0.12
	Ave.	0.13	0.09	0.08	0.13

Table 2: Results of graphite corrosion

From these results it is found that the average values of the three disks $\overline{\Delta r}_{cor,IPD}$ for all runs were nearly equal. This is not expected from a theoretical point of view, because higher graphite temperature should lead to a smaller depth of the corrosion attack. This discrepancy between the experimental results and the theory could possibly partly be explained by increasing surface erosion with increasing flow rates. Furthermore, usual diffusion models may be not valid, if the depth of the corrosion attack is in the same order of magnitude as a structure parameter (filler or pore diameter) of the porous solid.

A comparison between concentrations measured and calculated in produced and consumed gases is shown in Table 3. The concentrations of carbon dioxide and oxygen are calculated as follows:

$$C_{CO_2} = \frac{M_{CO_2}}{M_C} \cdot \frac{\Delta m_C}{\Delta t} \cdot \frac{1}{\dot{V}_t} \cdot 100 \qquad (3\text{-}7)$$

$$C_{O_2} = \frac{M_{O_2}}{M_C} \cdot \frac{\Delta m_C}{\Delta t} \cdot \frac{1}{\dot{V}_t} \cdot 100 \qquad (3\text{-}8)$$

Run		1	2	3	4
Total corroded mass of the graphite cylinder (kg)		0.481	0.398	0.363	0.312
Concentration of carbon dioxide ; C_{CO_2} (%)	(1)	0.36	0.20	0.20	0.10
	(2)	0.36	0.20	0.19	0.09
	(3)	0.30	0.22	0.20	0.08
Concentration of oxygen consumed ; C_{O_2} (%)	(1)	0.36	0.20	0.20	0.10
	(2)	0.36	0.20	0.19	0.09
	(3)	0.22	0.18	0.18	0.08

(1): Values calculated by using total corroded mass of the graphite cylinder

(2): Values calculated by using average corroded mass of three disks

(3): Values measured by mass spectrometer

Table 3: Comparison between concentrations measured and calculated in produced and consumed gases

Using these equations, the concentrations in line (1) and (2) of Table 3 are calculated; the total corroded mass of the graphite cylinder was used as Δm_c in the calculation of line (1), and the average corroded mass of three disks for the calculation of line (2). The concentration in line (3) is a value measured by the mass spectrometer. Carbon monoxide is not included in these calculations, because its concentration was very low, probably due to reaction (1-3). A small amount of carbon monoxide was only measured for Run 4 which has the lowest temperature. Except of Run (1), there is a sufficient agreement between calculated and measured concentration values.

3.2 Mass transfer in boundary layer

3.2.1 Mean mass transfer coefficients

Reynolds number and Sherwood number were evaluated from the equations:

$$Re_d = \frac{U_\infty \cdot \rho_{mix} \cdot d_h}{\mu_{mix}} \qquad (3\text{-}9)$$

$$Sh = \frac{\beta \cdot d_h}{D_{O_2/N_2}} \qquad (3\text{-}10)$$

where d_h denotes the diameter of the cylinder before the corrosion (that means, corrosion induced changes of the diameter are not included), the velocity U_∞ was calculated from the volume flow rate and the cross section of the inner test section tube, and D_{O_2/N_2} denotes the diffusion coefficient of oxygen in nitrogen. The film temperature T_f $(=(T_g+T_c)/2)$ and the pressure at the test section were used in evaluation of thermal properties. The latter were calculated by equations in Appendix B.0 condensed from the PRIAMUS computer code /29/. The mean mass transfer coefficient β_m was calculated from the corroded mass Δm_c of the graphite as follows:

$$\beta_m = \frac{\dot{m}_{O_2}}{\rho_{mix}(w_{O_2,\infty} - w_{O_2,w})} \qquad (3\text{-}11)$$

$$\dot{m}_{O_2} = \dot{m}_C \cdot \frac{M_{O_2}}{M_C} \cdot \frac{2+f}{2(1+f)} \qquad (3\text{-}12)$$

$$w_{O_2,\infty} = \left(\frac{P_{O_2}}{P_t}\right)_\infty \cdot \frac{\frac{M_{O_2}}{M_{N_2}}}{1-\left(1-\frac{M_{O_2}}{M_{N_2}}\right)\left(\frac{P_{O_2}}{P_t}\right)_\infty} \qquad (3\text{-}13)$$

$$\dot{m}_C = \frac{\Delta m_C}{\Delta t \cdot \pi \cdot d_h \cdot l} \qquad (3\text{-}14)$$

where f was given in Reference /10/ and its equation was given in Appendix A.0 $(p_{O_2}/p_t)_\infty$ was obtained from the oxygen concentration at the inlet of the test section. For mass transfer calculations in the BLMR, the oxygen concentration at the surface of the graphite cylinder $w_{O_2,w}$ was defined as zero.

Two kinds of Δm_c are defined by Eqs. (3-4) and (3-5). $\Delta m_c^{(1)}$ is equal to $\Delta m_c^{(2)}$ if there is no in-pore corrosion. The Sherwood number calculated from $\Delta m_c^{(1)}$ includes a small contribution of in-pore diffusion, even in BLMR, as mentioned in 3.1.2. In the following, Δm_c defined by Eq. (3-5) ($=\Delta m_c^{(2)}$) was used. This was done, because there was no method at hand to measure the local corroded mass necessary for calculations of the local Sherwood number on the basis of $\Delta m_c^{(1)}$ and realising that the differences between the two values lay in the range of the experimental uncertainties.

The relations between mean Sherwood numbers and Reynolds numbers in the present experiments are shown in Fig. 7. The correlation used in this figure was obtained experimentally by: R. Hilpert /30/ Eq. (3-15). According to this, the mean Nusselt number at a circular cylinder in crossflow of air is:

$$Nu_m = 0.615 \cdot Re_d^{0.466} \qquad (40 \leqslant Re_d \leqslant 4000) \qquad (3\text{-}15)$$

W.J.M. Douglas and S.W. Churchill /15/ proposed the correlations on the mean Nusselt number as follows:

$$Nu_m = 0.46 \cdot Re_d^{0.5} + 0.00128 \cdot Re_d \qquad (500 \leqslant Re_d \leqslant 250000) \qquad (3\text{-}16)$$

In the following, Equation (3-15) was used; but there is only a small difference between Nu_m of Eqs. (3-15) and (3-16) of about 10 % for the Reynolds numbers of the present experiments. Taking into consideration that the heat transfer coefficients are empirically proportional to the one third power of the Prandtl number Pr, Equation (3-15) can be rewritten by using the value of Pr for air (=0.71) in the following manner:

$$Nu_m = 0.689 \cdot Re_d^{0.466} \cdot Pr^{1/3} \qquad (3\text{-}17)$$

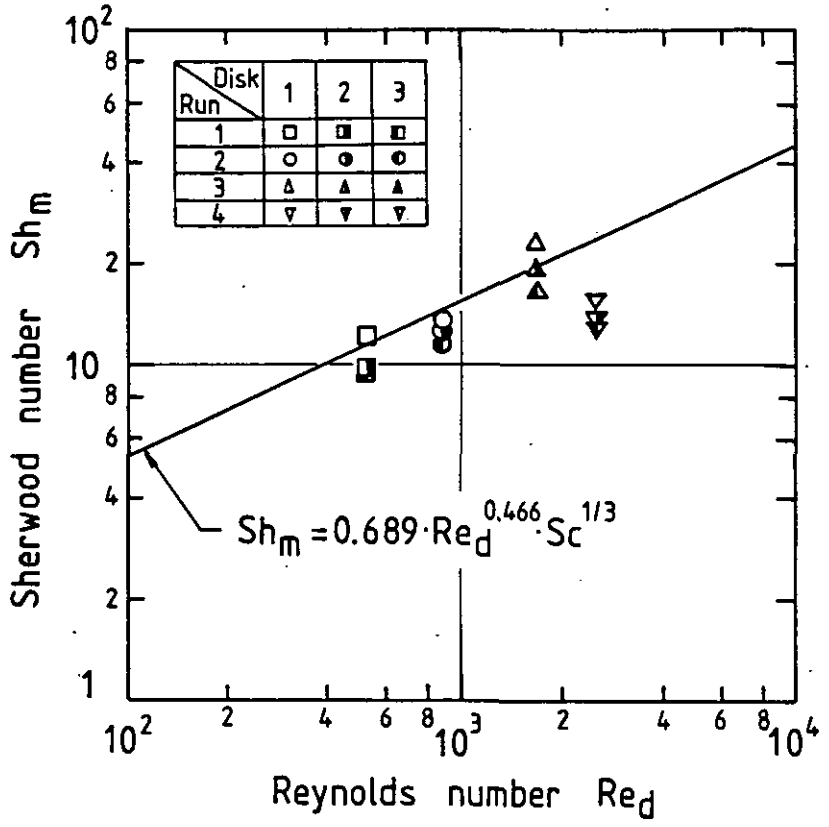

Fig. 7: Relation between mean Sherwood and Reynolds numbers

Furthermore, assuming that the analogy between the heat transfer and the mass tranfer applies as Pr/Sc is approximately 1, Equation (3-18) can be obtained from Eq. (3-17).

$$Sh_m = 0.689 \cdot Re_d^{0.466} \cdot Sc^{1/3} \qquad (3\text{-}18)$$

In Fig. 7 the experimental results in Runs 1 and 3 agree fairly well with Eq. (3-18). The mean Sherwood numbers of Runs 2 and 4 are smaller than those calculated by Eq. (3-18). This shows that Runs 2 and 4 were not in pure BLMR.

The results of the mass transfer in the present experiments can be correlated to the heat transfer data for uniform temperature distribution at the cylinder surface, which in case of mass transfer corresponds to a uniform oxygen concentration. The latter was defined as zero (see page 19). In contrast to the assumption of a constant concentration of $w_{O_2,\infty}$ used in these

calculations, the true value of $w_{O_2,\infty}$ varied by several percent around the cylinder. Therefore, the error of the mass transfer coefficients evaluated from the present experiments is increased by only a few percent due to this neglection.

The temperature distribution measured by the thermocouples in the cylinder was sufficiently uniform as expected. Maximum gas temperature rises calculated and measured between the inlet and the outlet of the test section were very small; therefore the above used assumption that the gas temperature is constant is nearly valid and no influence on the results of the mass transfer coefficient has to be expected by this assumption. A variation of the total gas pressure $(P_t)_\infty$ in Eq. (3-13) could principally have some influence, but the variation calculated according to Reference /31/ was very small. In Runs 1-3 the surfaces of the cylinder were smooth. Although the surface roughness of the upstream half of the cylinder after corrosion in Run 4 increased, Nikuradse's roughness paramter is so small that the results of the mass transfer in the present experiments can be regarded valid for the smooth surface.

3.2.2 Local mass transfer coefficients

Substituting $m_{O_2,\Theta}$ into Eq. (3-11), local mass transfer coefficients were evaluated. Using $\Delta m_{c,\Theta}$ defined as follows:

$$\boxed{m_{c,\Theta} = (V_{0,\Theta} \cdot \dot{V}_{cor,cal,\Theta}) \cdot \rho_{b,0}} \qquad (3\text{-}19)$$

$\dot{m}_{O_2,\Theta}$ was calculated from Eqs. (3-12)-(3-14) and (3-19). The subscript of Θ denoted that the value ranges from $(\Theta-\Delta\Theta/2)$ to $(\Theta+\Delta\Theta/2)$. Accordingly, the local Sherwood number Sh_Θ represented the value from the angle of $(\Theta-\Delta\Theta/2)$ to $(\Theta+\Delta\Theta/2)$.

The local Sherwood numbers around the cylinders of Runs 1-4 are shown in Figs. 8.1-8.4. In these figures the local Sherwood numbers were smoothly connected to make the profile of the local Sherwood numbers distinct. Only for Disk 1 the profiles of the local Sherwood numbers were not symmetric in all runs. As expected, the Sherwood numbers in run 4 were more uniform over the cylinder surface than in the other run (see page 27).

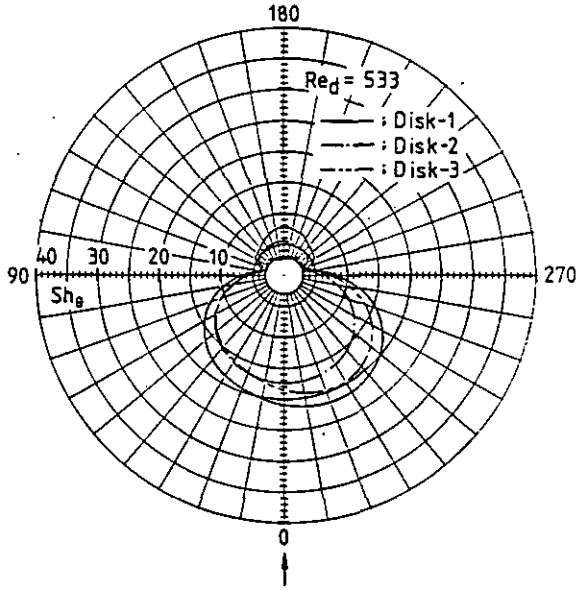

Fig. 8.1: Run 1

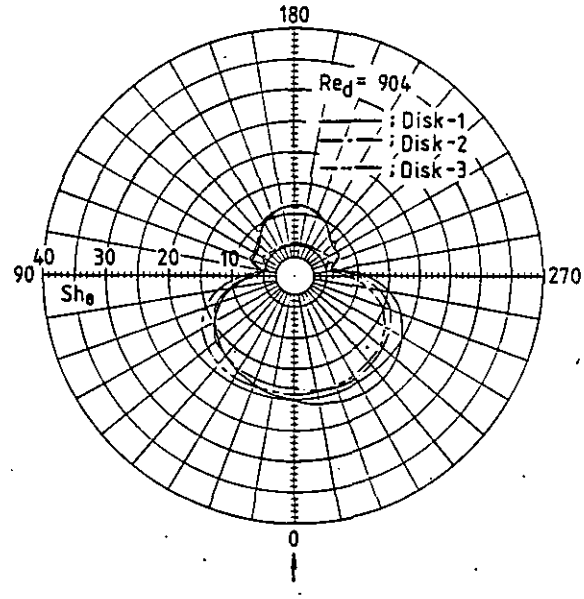

Fig. 8.2: Run 2

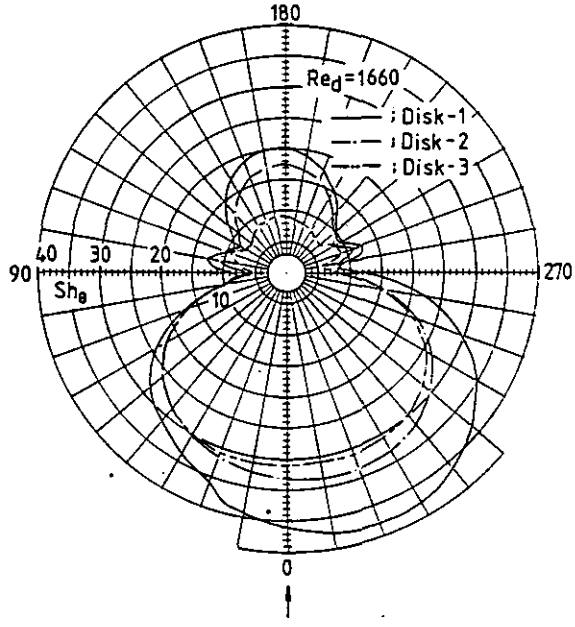

Fig. 8.3: Run 3

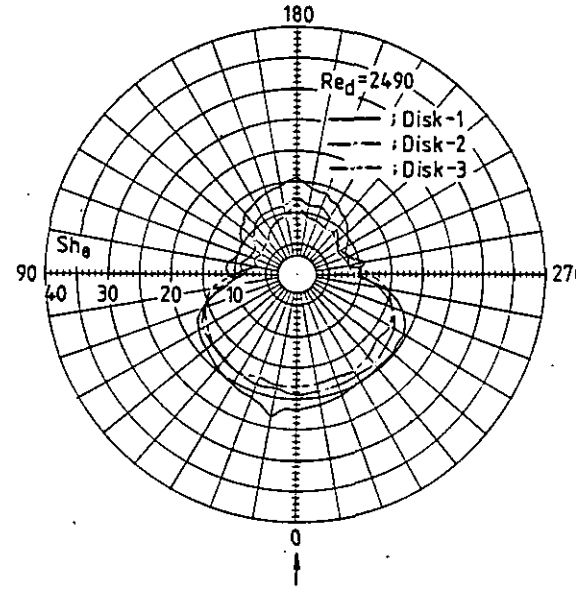

Fig. 8.4: Run 4

Fig. 8.1-8.4: Local Sherwood numbers around the cylinders

The ratios of the local Sherwood numbers to the mean Sherwood number around the cylinder for Disk-1 in Runs 1-4 are shown in Fig. 9. While Runs 1 and 3, which can be attributed to the BLMR, are in good agreement, the profiles of Run 2 and even more of Run 4 indicate the transition to the IPDR (see also Fig. 12).

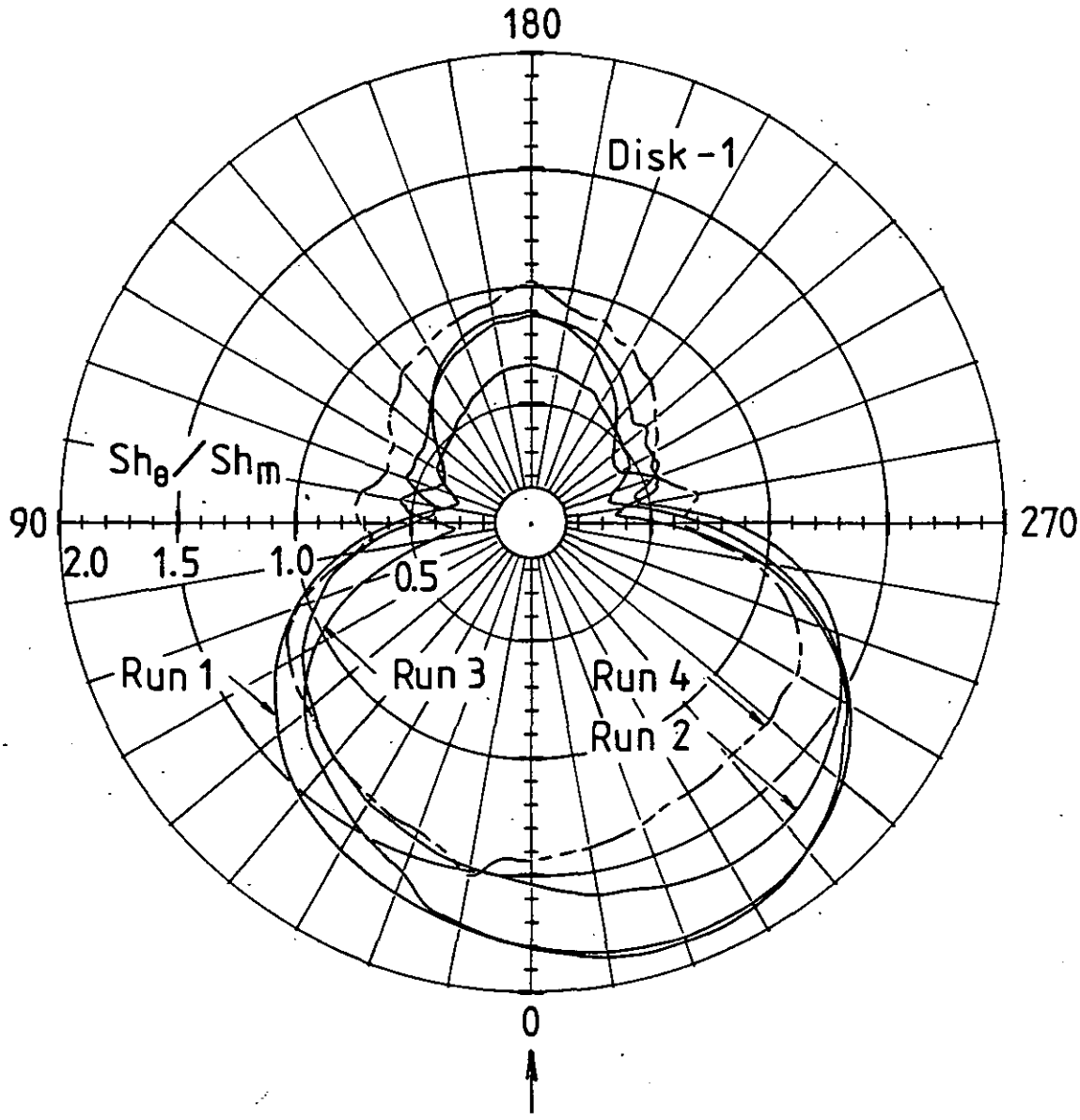

Fig. 9: Ratios of local Sherwood numbers to mean Sherwood number around a cylinder

Experimental results of other authors on the local heat transfer or the local mass transfer around a circular cylinder in crossflow are shown in Fig. 10. K.M. Krall and E.R.G. Eckert /20/ made the experimental study under the condition of uniform heat flux. They mentioned that the results

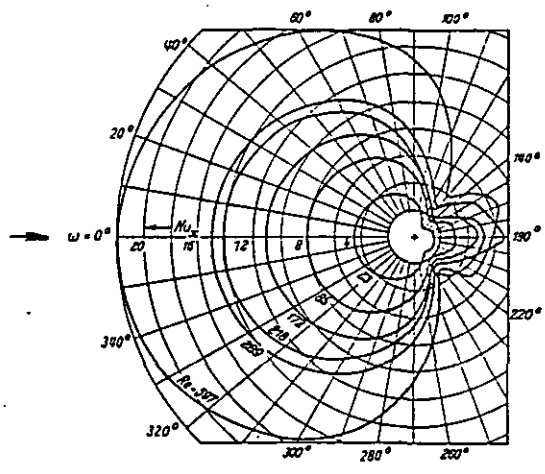

E.R.G.Eckert and E.Soehngen /13/

Re_d : 597, 289, 219, 172, 85, 23.

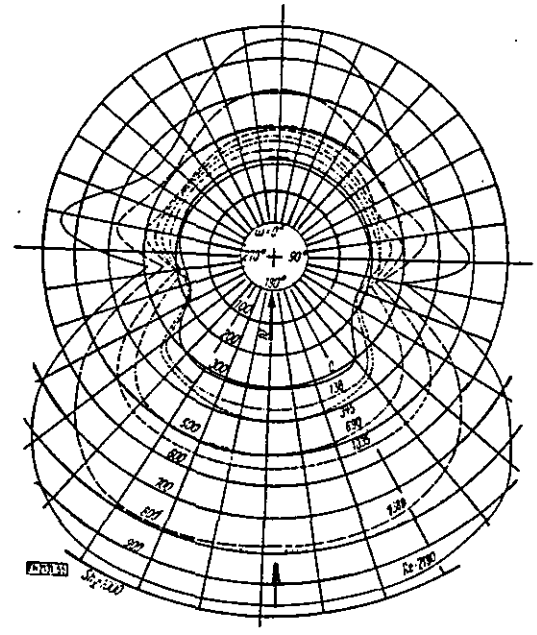

R.Wilhelm /32/

Re_d : 2180, 1380, 1035, 690, 345, 138, 0.

(Sc = 1760)

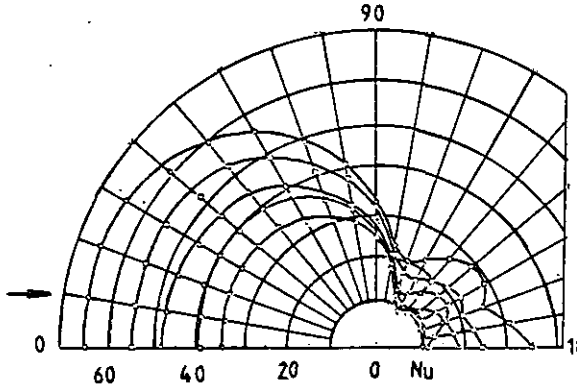

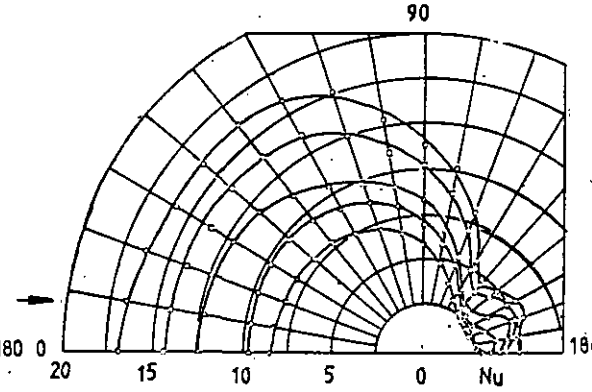

K.M.Krall and E.R.G.Eckert /20/

Re_d : 4640, 3570, 2830, 2140, 1630.

Re_d : 371, 281, 205, 138, 94.3.

Fig. 10: Experimental results on local heat or mass transfer around a cylinder in crossflow presented by other groups

on the heat transfer under uniform heat flux agreed well with those under uniform temperature; under this assumption and taking into account the above mentioned heat/mass transfer analogy the present results can be compared with their data. Figure 11 shows a direct comparison of the results of the local Sherwood numbers of Runs 1 and 3 with those of the local Nusselt numbers measured under similar conditions by /13/ res. /20/. In Fig. 11 the local Sherwood numbers were normalized by the mean Sherwood numbers and the local Nusselt numbers by Nu_m calculated from Eq. (3-15) or Eq. (3-17).

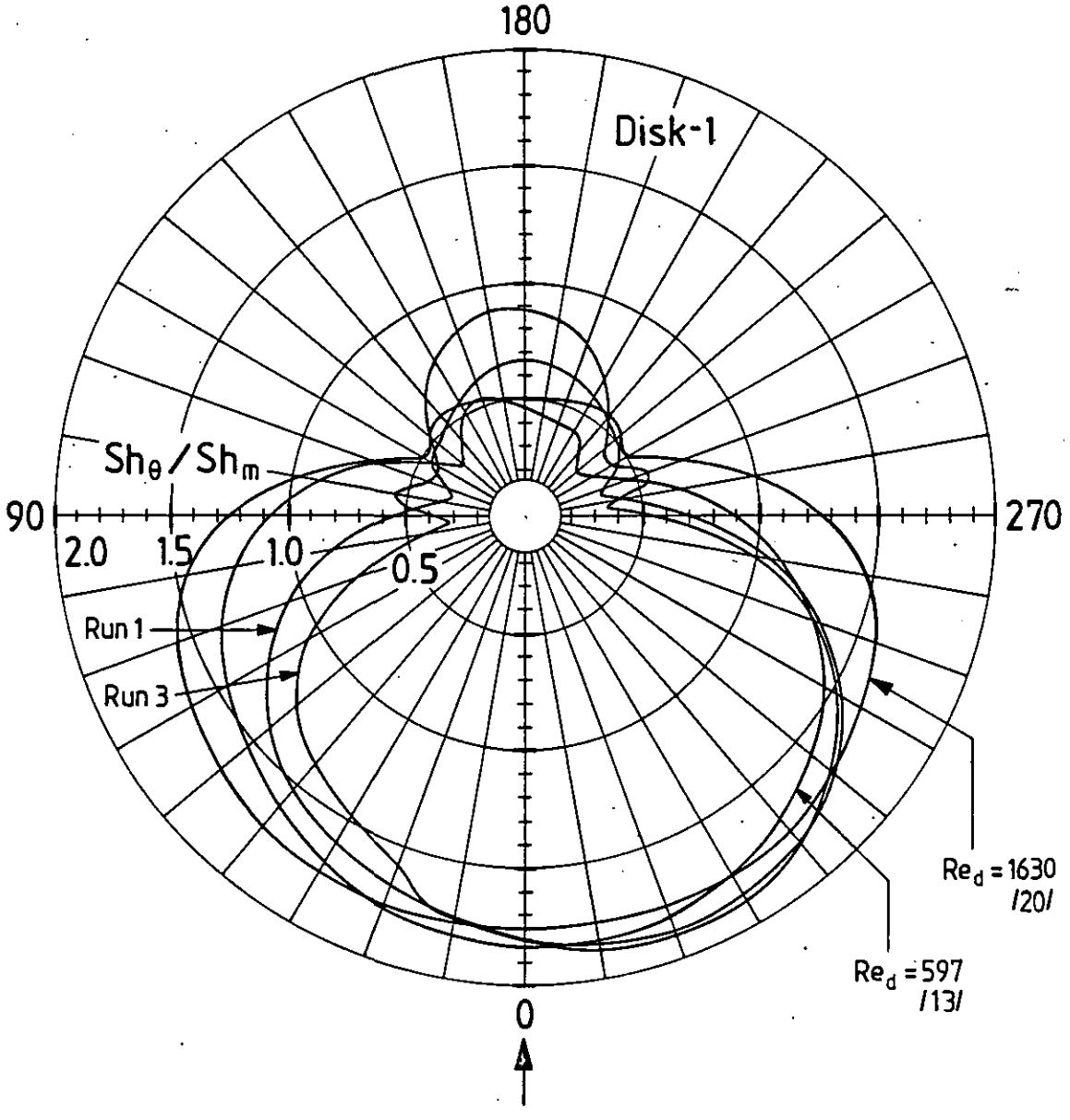

Fig. 11: Comparison of the present results on local Sherwood numbers with results on local Nusselt numbers

The agreement between both results was fairly good. From these comparisons of the present results on the mean and local Sherwood numbers with those of other experiments without chemical reactions it is concluded that the chemical reactions (1-1)-(1-3) do not have significant influences on the mass transfer.

The angles of the minimum of Sh_Θ, which correspond to the separation points, are listed in Table 4. In Runs 1-3 the angle of the separation point became smaller with increasing Reynolds number which is in line with the results of other authors shown in Fig. 10, especially with the results on the mass transfer of R. Wilhelm /32/.

Disk \ Run	1	2	3	4
1	106° -106°	98° -103°	86° -97°	89° -111°
2	105° -106°	101° -98°	89° -95°	94° -117°
3	108° -115°	105° -102°	93° -98°	121° -119°

Table 4: The angles between the separation points and the stagnation points

The maximum decrease of radius was about 6 mm (12 % of the radius before corrosion) and the average decreases of radii were less than 3.2 mm (6.4 %). In the case of such small changes in shape, the diameter of the cylinder before corrosion could be used for the hydraulic diameter in Eqs. (3-9) and (3-10). An effect of the change in shape on the mass transfer could not be detected under the actual conditions.

3.3 Mass transfer and in-pore diffusion

The corrosion rates of the graphite are given in Fig. 12. The broken lines show the corrosion rates of BLMR obtained by. Eq. (3-18) and dash-one-dotted lines are curves for IPDR, calculated by the following equation for the graphite material A3-3

$$\dot{m}_C = \frac{2.34 \cdot 10^{-2} \cdot \exp(-12850/T_K)(P_{O_2})_w}{1+0.00399 \cdot \exp(1569/T_K)\sqrt{(P_{O_2})_w}} \left(\frac{D_{O_2/N_2}}{D_{O_2/He}}\right)^{0.5} T_0 \qquad (3\text{-}20)$$

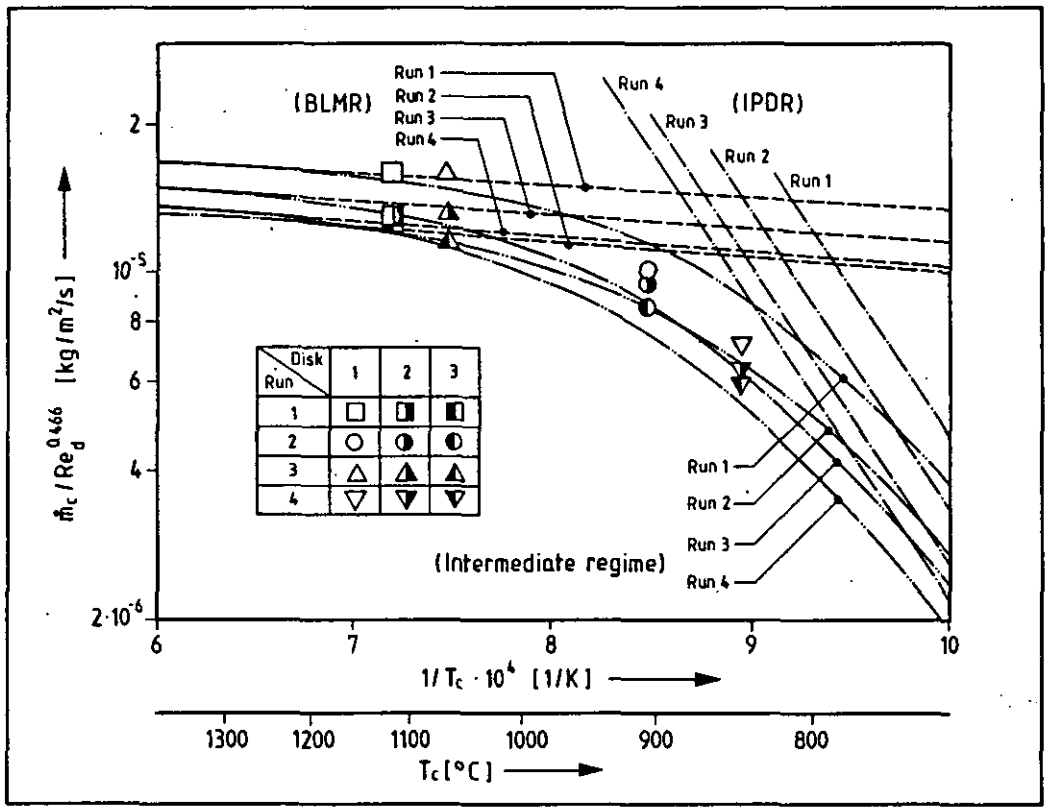

Fig. 12: Relation between corrosion rate and cylinder temperature

with $(P_{O_2})_w = (P_{O_2})_\infty$. The corrosion rate for the graphite material V483T was only slightly different from that of Eq. (3-20), as demonstrated in other experiments /33/. In the intermediate regime is valid: $0 \ll (P_{O_2})_w \ll (P_{O_2})_\infty$; the value of $(P_{O_2})_w$ necessary for calculation of the rate in this regime is obtained by solving the transcendent equation

$$0.012 \cdot \frac{\beta}{RT}\left((P_{O_2})_\infty - (P_{O_2})_w\right) = \dot{m}_C \qquad (3\text{-}21)$$

where the left-hand side represents mass-transfer and the right-hand side in-pore diffusion effects. In Fig. 12 dash-two-dotted lines show $\dot{m}_c$-values of the intermediate regime.

Because Run 1 and 3 agree fairly well with the BLMR-curves, it may be concluded, that these Runs were in pure BLMR; Run 2 seems to be influenced slightly and Run 4 strongly by in-pore diffusion. The dominating in-pore diffusion effect in Run 4 explains the higher uniform distribution of Sh_Θ for this Run (s. Fig. 9).

Korrekturen it Schreiben vom 5.Mrz.86 (Eing.)

4. CONCLUSION

The present experimental investigation on chemical reactions on a graphite cylinder with mass transfer and in-pore diffusion effects can be summarized as follows:

1. In the boundary layer mass transfer controlled regime (BLMR), the mean and local Sherwood numbers obtained in the present experiments agreed fairly well with the empirical relation of mass transfer Eq. (3-18) or - on the basis of the analogy between heat and mass transfer - with the results of the local Nusselt numbers by others.

2. The chemical reactions (eq. 1-1 to 1-3) did not have significant influence on the mass transfer. That means, that one basic assumption of the graphite corrosion code REACT/THERMIX / 4/ is valid and an increase of mass transfer by chemical reactions /26/ has not to be taken into account under HTGR air ingress accident conditions.

5. NOMENCLATURE

c_p	Specific heat constant pressure	(J/kg/K)
C	Concentration: C_{O2}, C_{CO}, C_{CO2}	(%)
D	Diffusion coefficient	(m^2/s)
	$D_{O2/He}$: Oxygen diffusion in helium atmosphere	
	$D_{O2/N2}$: Oxygen diffusion in nitrogen atmosphere	
d	Diameter of cylinder or disk	(m)
d_h	Hydraulic diameter	(m)
f	$= C_{CO}/C_{CO2}$	
h	Characteristic length of test section tube	(m)
l	Thickness of disk	(m)
M	Molecular weight	(g/mol)
	M_C = 12.010, M_{O2} = 32.000, M_{CO} = 28.010	
	M_{CO2} = 44.010, M_{N2} = 28.016	
m	Mass	(kg)
$\dot{m}_c$	Corrosion rate	(kg/m^2/s)
Δm	Corroded mass	(kg)
Nu	Nusselt number	
N	Mole number	(mol)
p	Pressure	(Pa)
p_{O2}	Partial pressure of oxygen in the mixture gas	(Pa)
Pr	Prandtl number	
Re_d	Reynolds number for cylinder	
Sc	Schmidt number	
Sh	Sherwood number	
T	Temperature in celsius	(°C)
T_k	Temperature in kelvin	(K)
Δt	Testing time period	(s)
U_∞	Flow velocity of free stream	(m/s)

V	Volume	(m^3)
$\dot{V}$	Volume flow rate	(m^3/s)
w	Mass concentration ratio, = $n_i M_i / n / M$	

(Greek Symbols)

β	Mass transfer coefficient	(m/s)
γ	Mass ratio	
θ	Angle from stagnation point	(deg)
λ	Thermal conductivity	(W/m/K)
μ	Viscosity	(Pa·s)
ρ	Density	(kg/m^3)

(Subscripts)

b	Bulk
C	Carbon
CO	Carbon monoxide
CO_2	Carbon dioxide
c	Cylinder
cal	Calculated value
cor	Value after corrosion
d	Diameter of cylinder or disk
f	Film
g	Gas
m	Mean value
mix	Value for gas mixture
ms	Measured value
O_2	Oxygen

t	Total value
w	Value on the wall
Θ	Local value
∞	Value in free stream
0	Value before corrosion
$-$	Mean or average value

6. REFERENCE

/ 1/ A. W. Barsell and M.B. Peroomian:
Consequences of Water Ingress into the HTGR Primary Coolant
GA-A 13171, (1975)

/ 2/ P. Kubaschewski and B. Heinrich:
Einfluß von Störfällen mit Wassereinbruch auf das Verhalten der Brennelemente im THTR-300
Proc. Reaktortagung 1978, Hannover, pp. 331-334, (1978)

/ 3/ M. Rossberg, E.Wicke:
Transportvorgänge und Oberflächenreaktionen bei der Verbrennung graphitischen Kohlenstoffs.
Chem.-Ing.-Techn. 28 (1956) 181

/ 4/ R. Moormann and K. Petersen:
REACT/THERMIX - Ein Computercode zur Berechnung der störfallbedingten Graphitkorrosion in Kugelhaufenreaktoren
Jül-1782, April (1982)

/ 5/ R. Moormann:
Graphite Oxidation Phenomena During Massive Air Ingress Accidents in Nuclear High Temperature Gas Cooled Reactors with Pebble Bed Core
Ber. Bunsenges. Phys.Chem. 87, pp. 1086-1090, (1983)

/ 6/ R. Moormann:
Effect on Delays in Afterheat Removal on Consequences of Massive Air Ingress Accidents in High-Temperature Gas Cooled Reactors
J. of Nucl.Sci.Tech., 21 (11), pp. 824-835, (1984)

/ 7/ R. Moormann, J. Anhalt, P. Ashworth, H.-K. Hinssen and W. Katscher:
Investigation of the Kinetics of the Interaction between Oxygen and Reactor Graphitic Materials
Proc. 5th London Int. Carbon and Graphite Conf., pp. 108-115, (1978)

/ 8/ W. Katscher, W. Delle, H.-K. Hinssen, R. Moormann and E. Wallura:
Changes in the Macroporosity of Nuclear Reactor Graphite Caused by Oxygen Corrosion
Proc. 3rd Baden-Baden Int. Carbon Conf., pp. 247-250, (1980)

/ 9/ W. Katscher, H.-K. Hinssen, R. Moormann, W. Delle and E. Wallura:
Changes in the Macroporosity of Nuclear Reactor Graphite under Oxygen Corrosion
High Temperature - High Pressure, Vol. 13, pp. 275-279, (1981)

/10/ H.-K. Hinssen, W. Katscher and R. Moormann:
Kinetik der Graphit/Sauerstoff-Reaktion im Porendiffusionsbereich.
Teil 1: Matrixmaterialien A3-3 und A3-27
Jül-1875, November (1983)

/11/ E.R. Gilliland and T.K. Sherwood:
Diffusion of Vapors into Air Streams
Ind. Eng. Chem., 26, p. 516, (1934)

/12/ E. Schmidt and K. Wenner:
Wärmeabgabe über den Umfang eines angeblasenen geheizten Zylinders
Forsch. Ing.-Wes., 12 (2), pp. 65-73, (1941)

/13/ E.R.G. Eckert and E. Soehngen:
Distribution of Heat-Transfer Coefficients Around Circular Cylinder in Crossflow at Reynolds Numbers from 20 to 500
Trans. ASME, 74, pp. 343-347, (1952)

/14/ S.W. Churchill and J.C. Brier:
Convective Heat Transfer from a Gas Stream at High Temperature to a Circular Cylinder Normal to the Flow
Chem. Engng. Progr. Symp.Ser., Vol. 51, No. 17, pp. 57-65, (1955)

/15/ W.J.M. Douglas and S.W. Churchill:
Recorrelation of Data for Convective Heat Transfer between Gases and Single Cylinder with Large Temperature Differences
Chem. Engng. Prog. Symp. Ser., Vol. 52, No. 18, pp. 23-28, (1956)

/16/ D.C. Collis and M.J. Williams:
Two-Dimensional Convection from Heated Wires at Low Reynolds Numbers
J. Fluis Mech., 6, pp. 357-384, (1959)

/17/ D.A. van Meel:
A Method for the Determination of Local Convective Heat Transfer from a Cylinder Placed Normal to an Air Stream
Int. J. Heat Mass Transfer, Vol. 5, pp. 715-722, (1962)

/18/ A.S. Grove, F.H. Shair, E.E. Petersen and A. Acrivos:
An Experimental Investigation of the Steady Separated Flow past a Circular Cylinder
J. Fluid Mech., 19, pp. 60-80, (1964)

/19/ R.M. Fand and K.K. Keswani:
A Continuous Correlation Equation for Heat Transfer from Cylinders to Air in Crossflow for Reynolds Numbers from 10^2 to $2x10^5$
Int. J. Heat Mass Transfer, Vol. 15, pp. 562-563, (1972)

/20/ K.M. Krall and E.R.G. Eckert:
Local Heat Transfer around a Cylinder at Low Reynolds Number
Trans. ASME, Ser. C, 95-2, pp. 273-275, (1973)

/21/ E. Achenbach:
Total and Local Heat Transfer from a Smooth Circular Cylinder in Crossflow at High Reynolds Number
Int. J. Heat Mass Transfer, Vol. 18, pp. 1387-1396, (1975)

/22/ M. Kawaguti and P. Jain:
Numerical Study of a Viscous Fluid Flow past a Circular Cylinder
J. Phys. Soc. of Japan, Vol. 21, No. 10, pp. 2055-2062, (1966)

/23/ J.S. Son and T.J. Hanratty:
Numerical Solution for the Flow around a Cylinder at Reynolds Numbers of 40, 200 and 500
J. Fluid Mech., Vol. 35, part. 2, pp. 369-386, (1969)

/24/ A.M. Petrie:
The Prediction of Heat Transfer in the Wake of Cylinder in Crossflow
Int. J. Heat Mass Transfer, Vol. 18, pp. 131-137, (1975)

/25/ P.C. Jain and B.S. Goel:
A Numerical Study of Unsteady Laminar Forced Convection from a Circular Cylinder
Trans. ASME, Ser. C, 98, pp. 303-307, (1976)

/26/ E. Specht and R. Jeschar:
Kopplung von Konvektion mit Chemischer Kinetik beim Abbrand von Kohlepartikeln
Ber. Buns. Phys. Chem., 87, pp. 1099, (1983)

/27/ R. Moormann and R. Finken:
Graphitkorrosionsuntersuchungen zu massiven Lufteinbruchstörfällen mit primärem Sauerstoffeintritt in die Säulenhalle am Beispiel des HTR-PNP-500
Proc. Jahrestagung Kerntechnik, Berlin 1983, pp. 203-206

/28/ B. Stauch:
SUPERNOVA, ein Experiment zur Untersuchung der Graphitkorrosion bei schweren Luft- und Wassereinbruchstörfällen in Kugelhaufen-HTR
KFA-ISF-IB-3/84, (1984)

/29/ R. Finken and R. Moormann:
PRIAMUS - Ein Rechenprogramm zur Bestimmung thermophysikalischer Stoffwerte von Gasmischungen aus O_2, N_2, CO, CO_2, He, H_2O, H_2 und CH_4
Jül-1916, Mai 1984

/30/ R. Hilpert:
Wärmeabgabe von geheizten Drähten und Rohren im Luftstrom
Forsch. Ing.-Wes. 4, p. 215, (1933)

/31/ JSME Data Book: Hydraulic Losses in Pipes and Ducts
Japan Society of Mechanical Engineers (in Japanese), (1979)

/32/ R. Wilhelm:
Der Stoffübergang fest-flüssig bei Einzelkörpern und Schüttungen in freier und erzwungener Strömung
VDI-Forsch., 531, Düsseldorf 1969

/33/ H.-K. Hinssen: Private communication

A.0 MOLE NUMBER RATIO OF CO TO CO_2

H.-K. Hinssen et al. /10/ proposed the experimental relations on the molal ratio of carbon monoxide to carbon dioxide.

$$f = C_{CO}/C_{CO_2} = a \cdot \exp(-b/T_k) \qquad \text{(A-1)}$$

where a = 500, b = 6059 at oxygen concentration of 1 %, a = 116, b = 4635 at 5 %, and a = 12.9, b = 2512 at 10 %, T_k was temperature in Kelvin. In the present report, values of 'a' and 'b' for the oxygen concentration from 1 % to 10 % in Eq. (A-1) were interpolated by the following equations.

$$a = 722.9 \cdot \exp(-35.17\ P_{O_2}/P_t) - 8.563 \qquad \text{(A-2)}$$

$$b = -7.622 \cdot (P_{O_2}/P_t)^2 - 3.103 \cdot (P_{O_2}/P_t) + 0.6377 \quad \times 10^4 \qquad \text{(A-3)}$$

B.0 THERMOPHYSICAL PROPERTIES OF THE GAS MIXTURES

For the temperature range between 800 and 1200°C the following simplified equations for the thermophysical properties of gas mixtures needed for mass/transfer calculations were used. They were obtained by means of the PRIAMUS code /29/. The error of the values calculated using there equations was within ± 1 % compared to PRIAMUS results.

(1) Density: ρ (kg/m^3)

$$\rho_i = A_i \frac{\rho}{T_K} \tag{B-1}$$

$$\rho_{mix} = \sum_{i=1}^{n} C_i \rho_i / 100 \tag{B-2}$$

(2) Thermal conductivity: λ (W/m/K)

$$\lambda_i = A_i \cdot T_K^{N_i} \tag{B-3}$$

$$\lambda_{mix} = \sum_{i=1}^{n} \frac{\lambda_i}{1 + \frac{100}{C_i} \sum_{i=1,j=1}^{n} C_i A_{ij} / 100} \tag{B-4}$$

$$A_{ij} = \frac{1}{4}\left(1 + \left[\frac{C_i}{C_j}\left(\frac{M_j}{M_i}\right)^{0.75} \cdot \frac{1 + S_i/T_K}{1 + S_j/T_K}\right]^{0.5}\right)^2 \cdot \frac{1 + S_{ij}/T_K}{1 + S_i/T_K} \tag{B-5}$$

$$S_{ij} = \sqrt{S_i S_j} \tag{B-6}$$

where S_{N_2} = 104, S_{O_2} = 127, S_{CO} = 101. S_{CO_2} = 253.

(3) Viscosity: μ (Pa·s)

$$\mu_i = A_i T_K^{n_i} \tag{B-7}$$

$$\mu_{mix} = \sum_{i=1}^{n} \frac{\mu_i}{1 + \frac{1}{C_i} \sum_{j=1,i=1}^{n} C_j \Phi_{ij}} \tag{B-8}$$

$$\Phi_{ij} = \frac{\left[1 + \frac{C_i}{C_j}\left(\frac{M_j}{M_i}\right)^{0.25}\right]^2}{\sqrt{8\left(1 + \frac{M_i}{M_j}\right)}} \tag{B-9}$$

(4) Specific heat at constant pressure: c_p (J/kg/K)

$$c_{p_i} = A_i T_K^{n_i} \tag{B-10}$$

$$c_{p_{mix}} = \sum_{i=1}^{n} Y_i c_{p_i} \tag{B-11}$$

(5) Prandtl number: Pr

$$Pr_i = \frac{c_{p_i} \cdot \mu_i}{\lambda_i} \tag{B-12}$$

(6) Schmidt number: Sc

$$Sc_i = \frac{\mu_i}{\rho_i \cdot D_{O_2/N_2}} \tag{B-13}$$

(7) Diffusion coefficient: $D_{O_2/N_2}(m^2/s)$

$$D_{O_2/N_2} = 1.716 \cdot 10^{-9} T_K^{1.675} \cdot 10^5 / P_t \tag{B-14}$$

In Eqs. (B-1)-(b-10) constants of A_i and n_i are listed in Tabel A-1.

Properties / Gas	ρ	λ		μ		c_p	
	$A_i \times 10^3$	$A_i \times 10^4$	n_i	$A_i \times 10^7$	n_i	A_i	n_i
Nitrogen	3.370	2.901	0.7735	4.266	0.6549	395.8	0.1567
Oxygen	3.849	5.078	0.7242	5.969	0.6363	499.6	0.1132
Carbon dioxide	5.293	1.899	0.8421	3.877	0.6648	367.9	0.1751
Carbon monoxide	3.369	3.539	0.7540	4.896	0.6427	429.1	0.1472

Table A-1: Constants of Eqs. (B-1)-(B-10) for thermal properties

ACKNOWLEDGEMENT

The authors want to express their gratitude to Dr. J. Fassbender, the former director of the Institut for Nuclear Safety Research (ISF) for his continuous encouragement and support of the present study. They also are obliged to Prof. E. Achenbach of the Institute for Reactor Components (IRB) for valuable discussions. They are grateful to Mr. H.-K. Hinssen and Mr. H. Seeboth for their assistance in carrying out the experiments and their valuable comments and guidanc in the data reduction. The authors also thank Mrs. Rath for typing the report and Mrs. Begemann for preparing the drawings.